Receptor-mediated cell attachment and detachment kinetics

I. Probabilistic model and analysis

Cindi Cozens-Roberts, Douglas A. Lauffenburger, and John A. Quinn
Department of Chemical Engineering, University of Pennsylvania, Philadelphia, Pennsylvania 19104 USA

ABSTRACT The kinetics of receptor-mediated cell adhesion to a ligand-coated surface play a key role in many physiological and biotechnology-related processes. We present a probabilistic model of receptor-ligand bond formation between a cell and surface to describe the probability of adhesion in a fluid shear field. Our model extends the deterministic model of Hammer and Lauffenburger (Hammer, D. A., and D. A. Lauffenburger. 1987. *Biophys. J.* 52:475–487) to a probabilistic framework, in which we calculate the probability that a certain number of bonds between a cell and surface exists at any given time. The probabilistic framework is used to account for deviations from ideal, deterministic behavior, inherent in chemical reactions involving relatively small numbers of reacting molecules. Two situations are investigated: first, cell attachment in the absence of fluid stress; and, second, cell detachment in the presence of fluid stress. In the attachment case, we examine the expected variance in bond formation as a function of attachment time; this also provides an initial condition for the detachment case. Focusing then on detachment, we predict transient behavior as a function of key system parameters, such as the distractive fluid force, the receptor-ligand bond affinity and rate constants, and the receptor and ligand densities. We compare the predictions of the probabilistic model with those of a deterministic model, and show how a deterministic approach can yield some inaccurate results; e.g., it cannot account for temporally continuous cell attachment or detachment, it can underestimate the time needed for cell attachment, it can overestimate the time required for cell detachment for a given level of force, and it can overestimate the force necessary for cell detachment.

INTRODUCTION

The kinetics of receptor-mediated cell attachment to and detachment from a surface, including other cells as well as biomaterials, is a central aspect of many physiological and biotechnology-related processes. For example, neutrophils are found in the bloodstream as nonadherent circulating cells; however, when tissue becomes infected, these cells migrate from the bloodstream into the tissue by first adhering to the endothelial cells (ECs) that line the blood vessel walls. This change in neutrophil attachment behavior, which is thought to be modulated by neutrophil "receptor" and/or EC "ligand" expression, is crucial because neutrophils provide the first line of defense against infection (1, 2). Biotechnology-related examples include certain cell separation techniques, such as cell affinity chromatography (CAC) (3–8), and EC seeding of prosthetic vascular grafts (9–15). In CAC, the cell mixture of interest is incubated with a ligand-coated surface (generally beads or membranes), the ligand being specific for receptors unique to the target cell (TC) population. After the incubation step, the strongly bound cells (principally TCs) are separated from the loosely bound and unbound cells by washing the surface. CAC has been proposed as an effective means of bone marrow purging for the removal of either tumor cells in autologous bone marrow transplantation (BMT) (6–8) or T-lymphocytes (T-cells) to reduce the incidence of graft vs. host disease (GVHD) in allogeneic BMT (5, 16). For this technique to be successful, TC removal must be virtually 100% efficient with minimal non-TC removal (7, 17). These criteria require an affinity surface that promotes TC attachment (with minimal non-TC attachment), and yields a TC-to-surface interaction that is strong enough to resist detachment during the wash step. EC seeding of vascular prosthesis has been proposed for small vessel replacements to overcome the thrombogenic nature of artificial graft materials because native blood vessels are lined with these cells. In addition, the seeding process reduces the incidence of graft infection (14, 15). It has been shown that coating the grafts with ligand that binds to specific EC receptors may improve seeding efficiencies (9, 10, 13). For this technique to be successful, the graft must support EC attachment and growth, as well as yield an adhesive interaction that is strong enough to resist detachment by shear stresses after implantation (9, 10, 13).

The adhesive force between a cell and a surface is the result of the net contribution of the nonspecific forces

Address correspondence to Prof. D. A. Lauffenburger, Department of Chemical Engineering, University of Pennsylvania, 220 South 33rd St., Philadelphia, PA 19104.

0006-3495/90/10/841/16 $2.00

(such as van der Waals, electrostatic, and steric stabilization) and the biochemically specific forces (receptor-ligand bonds) (18). The kinetics of the cell-to-surface interaction, therefore, depend on the cell and surface properties, the medium composition, and the external forces, such as the hydrodynamic force. Due to the complexity of this interaction, in vitro assays are typically used to study transient behavior (although in vivo experiments have been performed with implanted grafts [9, 15]). In general, attachment kinetic experiments are performed by incubating the cell and surface for a variable amount of time (the attachment time) and then subjecting the cell to a constant external force for a given amount of time. These experiments provide data on the percentage of adherent cells before and after exposure to the force as a function of attachment time. In general, detachment kinetic experiments consist of incubating the cell and surface for a given amount of time and then exposing the cell to a constant external force for a set period of time. Here, data are obtained on detachment as a function of time of exposure to the external force. The external force is typically exerted by either centrifugation (19) or hydrodynamic shear. The hydrodynamic shear assays can be divided into two categories. First, the qualitative assays are those in which the surface shear stress is produced by simply washing the surface (20, 21). Second, the quantitative assays are those in which the value of the surface shear stress can be determined, such as parallel plate (22), in vitro seeded graft (10, 12), and rotating disc assays (13).

The transient studies on cell attachment and detachment have provided useful data on receptor-mediated adhesion kinetics. In this paper, our objective is to develop a theoretical framework for the analysis of such transient data. Here, we focus on the role of receptor-ligand kinetics in yielding deviations from ideal, deterministic behavior. A deterministic model does not provide for fluctuations or deviations about the mean solution. Fluctuations are, however, inherent to some degree in chemical reactions, i.e., most kinetic data do not follow the deterministic solution exactly but fluctuate about it (23–25). This is especially true when the number of reacting molecules is relatively small, as is the case with cell surface receptor molecules. Deviations from ideal attachment and detachment behavior may, however, also result from heterogeneous cell properties, such as receptor number and class (7, 26, 27), and heterogeneous surface properties, such as the presence of several different proteins that each interact with unique cell receptors (28, 29). The lack of quantitative information on these heterogeneities, however, makes it difficult to interpret their role in cell adhesion behavior at this time.

Hammer and Lauffenburger (30) used a deterministic model to calculate the number of receptor-ligand bonds between a cell and an affinity surface in a shear field. A probabilistic model can be used to describe the behavior of a system that evolves probabilistically in time, accounting for fluctuations in the behavior (31–33). In this work, we extend the deterministic model of Hammer and Lauffenburger (30) to a probabilistic framework, in which the probability that a certain number of bonds exist is calculated. In other words, instead of using a deterministic conservation equation for the number of receptor-ligand bonds, a probabilistic conservation equation is used. We examine expressions appropriate for cell attachment in the absence of fluid stress and develop expressions for cell detachment in the presence of fluid stress as a function of key system parameters, such as the distractive fluid force, the receptor-ligand bond affinity and rate constants, and the receptor and ligand densities. We relate the increase in bond number with time for attachment to the increase in adhesive force with time and complete bond breakage over time to cell detachment over time. We compare probabilistic predictions with deterministic predictions to illustrate any significant differences between the two. A deterministic model has been previously shown to successfully interpret trends between different experiments as system parameters are varied (30) and to explain equilibrium detachment data with a model cell system (34), but it is unable to account for transient attachment and detachment data because of its "all-or-none" character. In the succeeding paper (hereafter referred to as "Part 2" [35]), we use our probabilistic model to analyze transient data obtained with a model cell system and the Radial-Flow Detachment Assay (34), and we compare the predictions of our model

NOMENCLATURE

a	Contact area radius (μm)
$A(\theta)$	Drift term of Fokker-Planck equation
$B(\theta)$	Diffusion term of Fokker-Planck equation
C	Number of receptor-ligand complexes
F	Force (dyn)
J	Probability current
k_b	Boltzman constant (J/molecule-K)
k_f^0	Forward rate constant (cm^2/min)
k_r	Reverse rate constant under conditions of flow (min^{-1})
k_r^0	Reverse rate constant (min^{-1})
K^0	Affinity constant (cm^2)
n	Number
N	Surface density (cm^{-2})
p	Probability density function
P	Probability
R_f	Number of unbound receptors within the contact area
R_T	Total number of receptors available for binding within the contact area
t	Time (min)
T	Temperature (K)

Subscripts

a	Attachment
b	Bond
c	Critical
ct	Critical-transient
C	Number of bonds
f	Free
F	Final
L	Ligand
m	Maximum
s	Steady state
T	Total
u	Unstable

Greek characters

α	Dimensionless force acting on the bonds
δ	$1/R_T$
γ	Range of the bond interaction (nm)
η	Dimensionless critical transient detachment time
κ	Dimensionless dissociation constant
θ	Dimensionless bond number
σ^2	Variance
τ	Dimensionless time
Ψ	Half-life divided by the maximum value for the half-life
ζ	No. of adherent cells after shear divided by no. before shear

with transient data on EC seeding of prosthetic vascular grafts, CAC, and cell adhesion reported from other assays. This comparison with experimental data demonstrates that the probabilistic model more faithfully represents observed behavior.

DEVELOPMENT OF MATHEMATICAL MODEL

In this section, we first review the deterministic approach to modeling receptor-ligand kinetics. For attachment, we develop a simple expression for the formation of bonds between cell receptors and a ligand-coated surface as a function of the dimensionless attachment time (τ_a) and the dimensionless receptor/ligand dissociation constant (κ). For detachment, we derive an expression for the number of bonds as a function of the dimensionless force acting on the bonds (α), the dimensionless time (τ), and κ. In addition, we develop an expression to examine the possible existence of a stable steady state solution representing adhesion as a function of α and κ. Next, we review the probabilistic approach to modeling chemical reactions. For attachment, we use the expressions developed by McQuarrie (23) for bond formation in solution to examine the mean bond number and variance as a function of τ_a and κ; and for detachment, we develop an expression for the effect of α, τ, and κ on the probability density function for bonds.

Deterministic model for receptor-ligand kinetics

For the present analysis, we make three simplifying assumptions which are also made by Hammer and Lauffenburger (30). First, the cell possesses only one receptor class available for binding to the ligand; therefore, the affinity and rate constants are constant. Second, the distribution of complexes is homogeneous within the contact area. Third, the ligand density (N_L) is much greater than the receptor density (N_R), so N_L remains approximately constant. In addition, we are choosing to neglect diffusion of additional receptors from other regions of the cell in this work.

For cell attachment in the absence of fluid stress, the deterministic conservation equation for the reaction between receptors on a cell surface and immobilized ligand is represented by:

$$dC/dt_a = k_f^0 N_L (R_T - C) - k_r^0 C, \quad (1)$$

where C is the number of receptor-ligand complexes, t_a is the attachment time, R_T is the total number of receptors available for binding within the contact area, and k_f^0 and k_r^0 are the forward and reverse rate constants, respectively. k_r^0/k_f^0 is the equilibrium dissociation constant, the reciprocal of the affinity constant, K^0.

For cell detachment in the presence of fluid stress, the hydrodynamic force exerted on the cell stresses the bonds with the surface, decreasing the duration of each interaction as well as the equilibrium bond density. Bell (36) models the effect of an external force (such as the hydrodynamic force) on the bonds by replacing k_r^0 by k_r, where:

$$k_r = k_r^0 \exp(\gamma F_T / k_b T C), \quad (2)$$

where F_T is the total force exerted on the bonds; γ is the range of the interaction; k_b is the Boltzman constant; and T is the temperature. This expression is based on the assumptions that nonspecific forces play a negligible role in countering the hydrodynamic force, the specific interaction involves only one receptor class, and the force per bond and bond density are uniform within the contact area. We substitute the expression in Eq. 2 into Eq. 1 for k_r^0 to develop the appropriate equation for detachment. F_T can be estimated with a force and torque balance, such as that developed by Hammer and Lauffenburger (30) for receptor-mediated cell adhesion with a spherical cell. Their model also assumes that the nonspecific adhesive force is negligible, one receptor class is available for binding, and the force per bond and bond density are

uniform. The stress distribution has also been modeled as a function of position within the contact area (37–39), with cell detachment occurring by "peeling" off of the surface, rather than as uniform, with cell detachment occurring when all of the bonds have broken. With "peeling," bonds in a given region are broken as the membrane in that region "peels" away from the surface; therefore, the probabilistic model would have even increased importance because fewer bonds need be described.

We define the following dimensionless parameters:

$$\theta = C/R_T \quad \tau_a = k_f^0 N_L t_a \quad \tau = k_f^0 N_L t$$
$$\kappa = k_r^0/k_f^0 N_L \quad \alpha = [\gamma/k_b T R_T] F_T,$$

where θ is the dimensionless bond number, τ_a is the dimensionless attachment time, τ is the dimensionless time, κ is the dimensionless dissociation constant, and α is the energy acting on the bonds scaled to the thermal energy, defined as the dimensionless force. This yields the attachment and detachment equations in dimensionless form:

$$d\theta/d\tau_a = (1 - \theta) - \kappa\theta \tag{3}$$

and

$$d\theta/d\tau = (1 - \theta) - \kappa\theta \exp(\alpha/\theta), \tag{4}$$

respectively. Eqs. 3 and 4 are deterministic equations because, given the value of θ at some dimensionless time (taken as the initial condition), the value at any other dimensionless time is fixed, with no apparent fluctuations or deviations about the values.

The initial condition for attachment is: $\tau_a = 0$, $\theta = 0$. This simply states that no bonds have formed at $t_a = 0$. We solve Eq. 3 for θ as a function of τ_a and obtain:

$$\theta = (1 + \kappa)^{-1}\{1 - \exp[-(1 + \kappa)\tau_a]\}. \tag{5}$$

The initial condition for detachment is obtained from the expression for θ (Eq. 5) evaluated at the appropriate value of τ_a. Eq. 4 is solved numerically, using the Runga-Kutta method (40). We define detachment as occurring when the bond number is equal to zero, i.e., when $\theta = 0$. Thus, when $\theta > 0$, all cells are attached, whereas when $\theta = 0$, no cells are attached. Clearly, this predicts "all-or-none" behavior for a homogeneous system.

The steady state analysis of detachment also provides some useful insight on the dynamic behavior. At steady state, Eq. 4 reduces to the following:

$$(1 - \theta) = \kappa\theta \exp(\alpha/\theta). \tag{6}$$

The left-hand side (lhs) of Eq. 6 is the dimensionless rate of bond formation and the right-hand side (rhs) is the dimensionless rate of bond breakage. For the steady state analysis, we plot the lhs and the rhs vs. θ for a given α and κ (see Fig. 1). From these plots, we are able to determine the number of steady states (the number of roots for Eq. 6) as well as the stability of the steady states. A stable steady state with $\theta > 0$ would represent adhesion. This information will provide a basis for understanding predictions of the deterministic model for cell adhesion behavior.

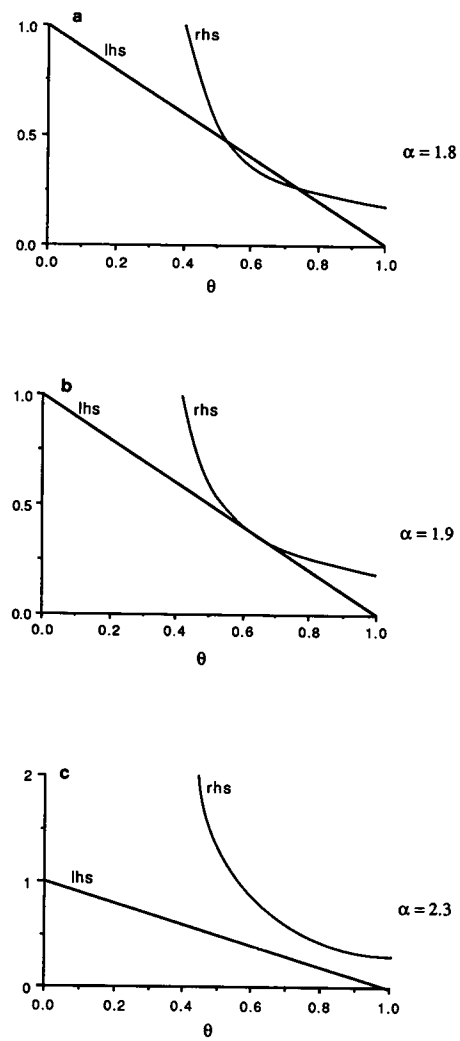

FIGURE 1 Results of the deterministic steady state analysis of detachment. Here, the dimensionless rate of bond formation (lhs of Eq. 6) and the dimensionless rate of bond breakage (rhs of Eq. 6) are plotted vs. the dimensionless bond number (θ) at $\kappa = 0.029$. (*a*) The dimensionless force (α) is equal to 1.8; (*b*) 1.9; and (*c*) 2.3.

Probabilistic model for receptor-ligand kinetics

Most kinetic data do not follow the deterministic solution exactly, but fluctuate about it (23–25). This is especially true when the number of reacting molecules is relatively small. Probabilistic modeling of chemical kinetics can be used to include the deviations about the values for the reactant(s) and product(s). We assume that the behavior of a system is Markovian, determined entirely by knowledge of the most recent condition, i.e., its future depends only on its present state and not on its past (31–33). A chemical reaction can best be modeled by a particular class of process called the birth–death process (23, 24, 32, 33). This process was originally used to study the fluctuations that exist in the number of individuals in a population with respect to time. We use the birth–death concept for chemical kinetics to develop a probabilistic description of the reaction between receptors on a cell surface and immobilized ligand. This seems appropriate a priori for two reasons. First, the total number of receptors on a cell is fairly small, roughly 10^3–10^7 (41). Second, transient experimental data exhibit temporally-continuous changes in state, rather than "all-or-none" behavior (see Part 2 [35]). Here, we again assume that the number of total receptors in the contact area is constant, the distribution of complexes is uniform, the ligand density is much greater than the receptor density, and the rate constants are constant.

We define $P_C(t)$ as the probability that there are C receptor-ligand bonds, or complexes, at time t. The probability that there are C complexes at time $t + \Delta t$ is given by the following:

$$\begin{aligned} P_C(t + \Delta t) = P_C(t) &\\ &+ k_f^0 N_L [R_T - (C - 1)] P_{(C-1)}(t) \Delta t \\ &- [k_f^0 N_L (R_T - C) P_C(t) \Delta t \\ &+ k_r^0 C P_C(t) \Delta t] \\ &+ k_r^0 (C + 1) P_{(C+1)}(t) \Delta t \\ &+ 0 [(\Delta t)^2], \end{aligned} \tag{7}$$

where Δt is a small step of time. The second term on the rhs of Eq. 7 represents the probability of having $(C - 1)$ complexes at t and adding one during Δt; the third and fourth terms are the probability of having C complexes at time t and adding one or losing one during Δt, respectively; and the fifth term represents the probability of having $(C + 1)$ complexes at t and losing one during Δt. Notice that this expression is for bond formation in the absence of stress. We take the limit in Eq. 7 as $\Delta t \rightarrow 0$ to obtain the so-called Master equation for the probability of a given number of bonds (Appendix 1). This provides us with $R_T + 1$ coupled ordinary differential equations.

McQuarrie (23) uses the method of generating functions with the Master equation for a reversible first-order reaction in solution to derive expressions for the mean number of reactant and for the variance as a function of time. The Master equation used by McQuarrie is identical to that for cell attachment in the absence of fluid stress. Therefore, we rearranged his results to yield the following expressions for the mean bond number ($\langle\theta\rangle$) and for the variance in bond number (σ^2) as a function of τ_a:

$$\langle\theta\rangle = (1 + \kappa)^{-1} \{1 - \exp[-(1 + \kappa)\tau_a]\} \tag{8}$$

and

$$\begin{aligned} \sigma^2 = (1 + \kappa)^{-2} (\kappa \{1 - \exp[-(1 + \kappa)\tau_a]\} \\ + \exp[-(1 + \kappa)\tau_a] - \exp[-2(1 + \kappa)\tau_a]), \end{aligned} \tag{9}$$

respectively. This expression for $\langle\theta\rangle$ is identical to that for θ from the deterministic attachment model (Eq. 5). For the deterministic model, however, σ^2 does not exist because no fluctuations about the values are allowed. At steady state, Eq. 8 and Eq. 9 reduce to:

$$\langle\theta\rangle = \langle\theta\rangle_s = (1 + \kappa)^{-1} \tag{10}$$

and

$$\sigma^2 = \sigma_s^2 = \kappa/(1 + \kappa)^2, \tag{11}$$

respectively, where $\langle\theta\rangle_s$ is the steady state value of $\langle\theta\rangle$ and σ_s^2 is the steady state value of σ^2.

For cell detachment in the presence of fluid stress, we simply substitute the expression for k_r (Eq. 2) into Eq. 7 for k_r^0 and take the limit as $\Delta t \rightarrow 0$ to obtain the Master equation. We put the Master equation in dimensionless form; take the limit as $\delta \rightarrow 0$, where $\delta = 1/R_T$ (a reasonable approximation for $R_T \gg 1$); and expand the probabilities and the exponential part of the reverse rate constant in a Taylor's series about P_θ and $\exp(\alpha/\theta)$, respectively (Appendix 1). The resulting equation is a Fokker-Planck equation, which gives the time evolution of the probability density function, $p(\theta, \tau)$, for the system (31–33), where p is a density of probability measure of the event for the event space (the range of θ that is of interest) (42). The Fokker-Planck equation can be written in the form:

$$\partial p/\partial\tau = -\partial/\partial\theta [A(\theta) p] + (1/2)\partial^2/\partial\theta^2 [B(\theta) p], \tag{12}$$

where:

$$A(\theta) = (1 - \theta) - \kappa\theta \exp(\alpha/\theta) \tag{13}$$

and

$$B(\theta) = [(1 - \theta) + \kappa\theta \exp(\alpha/\theta)]\delta. \quad (14)$$

The Fokker-Plank equation can also be written in the form:

$$\partial p/\partial\tau + \partial J/\partial\theta = 0, \quad (15)$$

where J is the probability current (33) (Appendix 1).

The initial condition for Eq. 12 is obtained from the expressions for $\langle\theta\rangle$ and σ^2 evaluated at the appropriate value of τ_a (Eqs. 8 and 9). At $\theta = 1$, there is a reflecting barrier, a result of the fact that probability cannot leave the event space, i.e., there can never be greater than R_T bonds ($\theta > 1$). Therefore, the boundary condition at $\theta = 1$ states that the net flow of probability across this barrier is zero:

$$J(1, \tau) = 0.$$

Both $A(\theta)$ and $B(\theta)$ are discontinuous at $\theta = \delta$; nevertheless, there is free motion across this point. This discontinuity is a result of the fact that a bond cannot be broken if there is no bond to break (which is the case between $\theta = 0$ and $\theta = \delta$). Because the probability and the current must be continuous across $\theta = \delta$, the boundary condition is (Appendix 1):

$$0 = \delta^2[\partial p(\delta, \tau)/\partial\theta] - [\alpha - 3\delta]p(\delta,\tau). \quad (16)$$

The Fokker-Planck equation for detachment is solved numerically, using a predictor-corrector method (43, 44). This solution technique introduces $p(0, \tau)$, which is assumed to be equal to zero, i.e., $\theta = 0$ is assumed to be "absorbing" (33). Physically, this means that once all of the bonds have been broken, a cell detaches and is unable to reattach. For consistency with this formulation, it is important that the initial condition include the point $p(0, 0) = 0$. A normal (Gaussian) distribution with the mean and variance predicted by Eqs. 8 and 9 predicts positive values for $p(0, 0)$; therefore, we use a lognormal distribution (45) with the same mean and variance. We recognize that the use of this distribution could affect the quantitative results; however, in general, it should not affect the qualitative behavior. One exception is the lognormal distribution cannot accurately describe the detachment behavior when the initial probability at small θ is significant (as is the case for large κ and/or small τ_a [see Eqs. 8 and 9]). On the other hand, when the initial probability at small θ is negligible (as is the case for small κ and/or large τ_a), $p(0, 0)$ can be set equal to zero in the normal distribution. Here, results obtained with the normal and with the lognormal distributions are identical.

The numerical results give the distribution of the probability density function from $\theta = \delta$ to $\theta = 1$ as a function of τ, κ, and α. The probability of any event is found by integrating the probability density function for the event over the event space (42). In other words, the area under the curve for the distribution from $\theta = \delta$ to $\theta = 1$ provides the value for the probability of having bonds (P_b), which we define to be the probability of the cell remaining attached. This area is obtained by numerical integration, using Simpson's rule (46).

GENERAL MODEL RESULTS

In this section, we present the results of the probabilistic and deterministic analyses of attachment and detachment. Throughout this section, the probabilistic predictions are compared and contrasted with the deterministic predictions. We show that the deterministic approach can yield some inaccurate results; e.g., it can underestimate the time required for cell attachment, it can overestimate the time required for cell detachment for a given level of force, and it can overestimate the force necessary for cell detachment. In addition, a deterministic model cannot account for temporally continuous cell attachment or detachment behavior. Ranges of the various parameter values, taken from some literature sources, are shown in Table 1.

Attachment

The probabilistic attachment model predicts $\langle\theta\rangle$ (Eq. 8) and σ^2 (Eq. 9) as a function of τ_a and κ. The deterministic attachment model predicts θ (Eq. 5), where θ is equal to $\langle\theta\rangle$, but does not allow for fluctuations about θ ($\sigma^2 = 0$). In Fig. 2, we illustrate the change in $\langle\theta\rangle$ with τ_a for κ equal to 0.0029, 0.029, and 0.29. The plots in Fig. 2 show three trends. First, at small values of τ_a, $\langle\theta\rangle$ increases

TABLE 1 Estimated parameter values

Parameter	Symbol	Range for cells
Receptor number/cell	R_{TC}	10^3–10^7 (41)
Ligand density	N_L	10^{10}–10^{12} cm^{-2} (49)
Bond number	C	0–3,000 (47, 50)
Affinity constant	K^0	10^{-11}–10^{-5} cm^2 (41)
Forward rate constant	k_f^0	10^{-11}–10^{-8} cm^2/s*
		10^{-14}–10^{-11} cm^2/s‡
Reverse rate constant	k_r^0	10^{-4}–10^{-2} s^{-1} (54)
Range of interaction	γ	0.5 nm (36)
Fluid force	F_T	0–10^{-3} dyn (37)
Attachment time	t_a	0–120 min (6, 13, 21)
Temperature	T	273–310 K

*For a diffusion-limited ligand-receptor interaction (51), where the lateral translational diffusion coefficient (D) of the receptor is typically between 10^{-11}–10^{-8} cm^2/s (52).

‡Smaller values are seen when the receptor-ligand interaction is not diffusion limited (53).

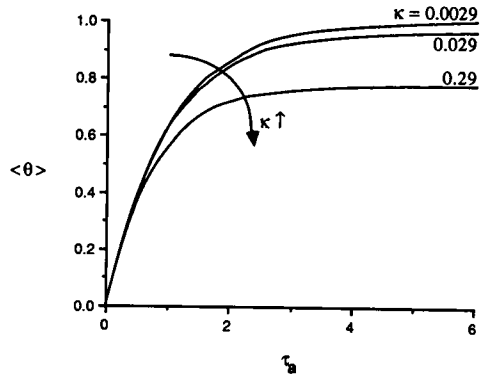

FIGURE 2 Results of the probabilistic attachment model. Here, we show a plot of the dimensionless mean bond number ($\langle\theta\rangle$) vs. the dimensionless attachment time (τ_a) at various values of the dimensionless dissociation constant (κ).

with τ_a. Second, at large τ_a, steady state is established, i.e., $\langle\theta\rangle = \langle\theta\rangle_s$. Third, as κ increases, $\langle\theta\rangle_s$ decreases, consistent with Eq. 10. The change in σ^2 with τ_a is illustrated in Fig. 3 for the values of κ in Fig. 2. The plots in Fig. 3 show three trends. First, σ^2 increases then decreases with τ_a. The simplest explanation for this trend is: at $\tau_a = 0, \theta = 0$ for all of the cells, whereas at larger τ_a, $\theta = \theta_s$ for most of the cells. Therefore, the initiation of bond formation results in an early increase in σ^2, and the approach to steady state results in a later decrease in σ^2. Second, at large τ_a, σ^2 reaches steady state, i.e., $\sigma^2 = \sigma_s^2$. Third, as κ increases, σ_s^2 increases, consistent with Eq. 11.

In this analysis, the decrease in κ could result from an increase in $k_f^0 N_L$ and/or a decrease in $k_r^0 \cdot \kappa^{-1}$ and τ_a are not independent, both are linearly proportional to $k_f^0 N_L$. Therefore, if k_r^0 remained constant and $k_f^0 N_L$ varied, t_a would be inversely proportional to $k_f^0 N_L$ at a given τ_a. As a result, plots of $\langle\theta\rangle$ vs. t_a and of σ^2 vs. t_2 would look different than those in Figs. 2 and 3, respectively. For example, for $k_f^0 N_L$ equal to 0.07, 0.7, and 7 min^{-1} (with k_r^0 equal to 0.02 min^{-1}), τ_a equal to 1 is equivalent to a t_a of ~14, 1.4, and 0.14 min, respectively. Therefore, as κ decreases, the initial rate of increase in $\langle\theta\rangle$ increases, and steady state is reached sooner (see Fig. 4). Correspondingly, as κ decreases, the initial rate of increase in σ^2 increases, with steady state reached sooner (not shown). If, however, k_r^0 varied and $k_f^0 N_L$ remained constant, t_a would be the same at a given τ_a, regardless of the value of κ. Therefore, plots of $\langle\theta\rangle$ vs. t_a and of σ^2 vs. t_2 would have the same features as those in Figs. 2 and 3, respectively.

A cell can be considered to be currently attached to a surface when $\theta \geq \delta$, i.e., when at least one bond exists. In Fig. 5, we compare the deterministic and probabilistic predictions for the fraction of adherent cells (ζ) as a function of τ_a at $\kappa = 0.029$. For the probabilistic analysis, ζ is calculated using a normal distribution with the values of $\langle\theta\rangle$ and σ^2 predicted by Eqs. 8 and 9, respectively. These two analyses show very different attachment behavior. First, the deterministic model predicts that there is a dimensionless time lag of $\sim 8 \times 10^{-4}$ before the onset of adhesion, whereas a portion of cells are predicted to attach almost instantaneously in the probabilistic model. Given estimates of $k_f^0 N_L$ in the range of 10^{-2}–10^6 min^{-1} (see Table 1) though, the deterministic lag should most often be negligible. Second, all of the cells attach ($\zeta = 1.0$) at the same value of τ_a in the deterministic model, a result of the fact that there are no fluctuations about θ. In the probabilistic model, however, ζ increases rapidly at first

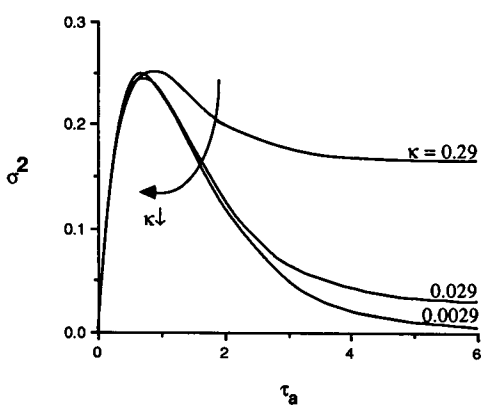

FIGURE 3 Results of the probabilistic attachment model. The variance (σ^2) is plotted as a function of the dimensionless attachment time (τ_a) at different values of the dimensionless dissociation constant (κ).

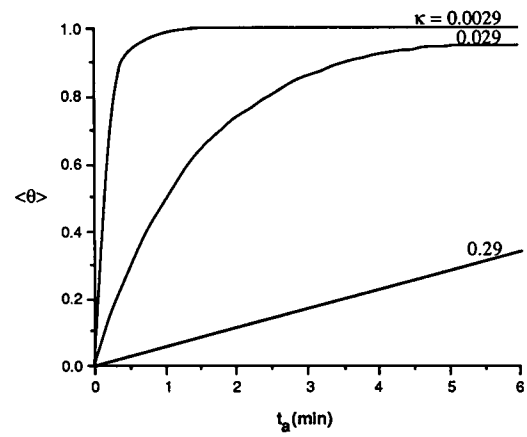

FIGURE 4 Results of the probabilistic attachment model. Here, we show a plot of dimensionless mean bond number ($\langle\theta\rangle$) vs. dimensional attachment time (t_a) at different values of the dimensionless dissociation constant (κ), where a change in κ is assumed to be the result of a change in the forward rate constant (k_f^0) and/or the ligand density (N_L). For these analyses, $k_f^0 N_L$ is equal to 0.07, 0.7, or 7 min^{-1} and k_r^0 is equal to 0.02 min^{-1} (κ is equal to 0.29, 0.029, or 0.0029, respectively).

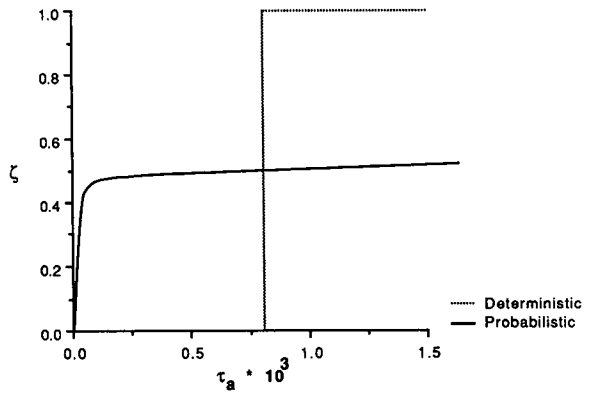

FIGURE 5 Results of the deterministic and probabilistic analyses of attachment. Here, we compare plots of the fraction of adherent cells (ζ) as a function of dimensionless attachment time (τ_a) for a dimensionless dissociation constant (κ) of 0.029. A cell is considered to be currently attached to the surface when at least one bond exists.

and then slowly as τ_a increases. This behavior can be attributed to the rapid increase in σ^2 at small τ_a (see Fig. 3). Initially, σ^2 and $\langle\theta\rangle$ are both small, so the dimensionless rate of increase in ζ is large. Then, σ^2 increases rapidly and $\langle\theta\rangle$ is still relatively small, so we see a decrease in the dimensionless rate of increase in ζ. Eventually (at $\tau_a \approx 2.0$), the probabilistic model predicts $\zeta = 1.0$. This difference in attachment behavior indicates that the deterministic approach underestimates the attachment time required for all of the cells to become attached to the surface. The magnitude of the underestimate again depends on the value of $k_f^0 N_L$, but it can be significant at the small end of the range. For example, for τ_a equal to 8×10^{-4} and 2.0, $k_f^0 N_L \approx 10^{-2}\ \text{min}^{-1}$ is equivalent to t_a of 0.08 and 200 min, respectively; however, $k_f^0 N_L \approx 10^6\ \text{min}^{-1}$ corresponds to t_a of 8×10^{-10} and 2×10^{-6} min, respectively, both of which are negligible.

Detachment

We are particularly interested in interpreting experimental data on the time-dependent detachment of a given cell type from a given surface over a range of shear stresses. In a given experiment, we assume that k_r^0, k_f^0, N_L, γ, T, and R_T are constant; therefore, α is linearly proportional to F_T. Consequently, we can analyze a given experiment with the probabilistic model by examining how $p(\theta)$ and P_b change with τ at various values of α for a fixed set of parameters. In addition, we can use the deterministic analysis to examine the change in θ with τ as well as the existence and stability of the steady states at various values of α for this same fixed set of parameters.

Unless otherwise stated, in the following analyses, we assume that $\kappa = 0.029$. For $R_T \gg 10$, the results as presented (in dimensionless form) are not a function of R_T because $\delta \ll 1$. F_T is linearly proportional to R_T for a given α at constant T and γ. Therefore, a change in R_T simply changes the value of F_T used in the analyses. In addition, unless otherwise stated, the initial condition for detachment is evaluated at $\tau_a = 2.0$. For the deterministic model with $\kappa = 0.029$, this gives $\theta(0) = 0.84$ (Eq. 5); and for the probabilistic model, this gives an initial probability distribution ($p[\theta, 0]$) with $\langle\theta\rangle = 0.84$ and $\sigma^2 = 0.13$ (Eqs. 8 and 9, respectively).

Deterministic analysis

A stable steady state is defined as θ_s, and an unstable steady state as θ_u. Typical results for the effect of α on θ_s and θ_u are illustrated in Figs. 1, *a–c* for α equal to 1.8, 1.9, and 2.3, respectively. Each figure consists of a plot of the lhs and of the rhs of Eq. 6 vs. θ, where the lhs is the dimensionless rate of bond formation and the rhs is the dimensionless rate of bond breakage. In Figs. 1, *a–c*: θ_u is 0.52, 0.62, and nonexistent, respectively; and θ_s is 0.77, 0.69, and nonexistent, respectively. Figs. 1, *a* and *b* can be divided into three regions. First, for $\theta_s < \theta \leq 1.0$, the magnitude of the rhs is greater than that of the lhs; therefore, the "driving force" is toward bond breakage. As a result, if θ started in this region ($\theta_s < \theta[0] \leq 1.0$), the value of θ would decrease as τ increased, and eventually a stable steady state would be established for which $\theta = \theta_s$. Second, for $\theta_u < \theta < \theta_s$, the magnitude of the lhs is greater than that of the rhs; therefore, the "driving force" is toward bond formation. If θ started in this region, the value of θ would increase with τ until $\theta = \theta_s$. Third, for $0 < \theta < \theta_u$, the rhs is greater than the lhs. Therefore, if θ started in this region, the value of θ would quickly drop with τ until $\theta = 0$. We assume that a cell detaches from the surface when $\theta = 0$. Fig. 1 *c* consists of only one region, equivalent to the third region in Figs. 1, *a* and *b*; therefore, there are no steady states. Here, regardless of $\theta(0)$, the value of θ drops with τ until $\theta = 0$.

Zero is the only value of α that gives a single steady state that is stable. For $\alpha > 0$, there are either two steady states (one stable and one unstable), one unstable steady state, or no steady states. From Figs. 1, *a* and *b*, we see that as α increases, θ_u increases, and θ_s decreases. As a result, the size of the second region decreases, whereas the first and third regions increase. Eventually $\theta_u = \theta_s$, and, at this value of α, defined as the critical value of α (α_c), there is no longer a stable steady state. For $\alpha > \alpha_c$, there are no steady states (stable or unstable). If $\theta(0)$ is greater than or equal to the value of θ at which $\theta_u = \theta_s$, then: for $\alpha < \alpha_c$, θ changes with τ until $\theta = \theta_s$; and, for $\alpha \geq \alpha_c$, θ decreases with τ until $\theta = 0$. If $\theta(0)$ is less than the value of θ at which $\theta_u = \theta_s$; then all of the cells remain adherent until the value for α at which $\theta(0) = \theta_u$. For this value of α and greater, all of the cells detach. Typically, however, $\theta(0) \geq$

$\theta(\theta_u = \theta_s)$, and, unless otherwise stated, we assume this to be the case. As a result, a plot of ζ_F (the "final" fraction of adherent cells) vs. α is a step function, with $\zeta_F = 1.0$ for $\alpha < \alpha_c$ and $\zeta_F = 0$ for $\alpha \geq \alpha_c$.

In Fig. 6, results for the fraction of adherent cells (ζ) as a function of τ are shown at several values of α. Values of α around 2 correspond to a force, F_T, of roughly 4×10^{-4} dyn, for typical values of related parameters, $\gamma = 0.5$ nm, $T = 310$ K, and $R_T = 250$ (recall, this is receptors/contact area, assuming no accumulation due to diffusion from other regions of the cell). This value for the force is on the order of that acting on a white blood cell adhering to a blood vessel wall (37). As mentioned, we define cell detachment as occurring when all of the bonds have broken (when $\theta = 0$). The plots in Fig. 6 show several interesting trends. First, ζ remains at one at the lower range of α and drops to zero at the higher range of α. This is consistent with the steady state analysis which predicts that $\zeta_F = 1.0$ for $\alpha < \alpha_c$ and $\zeta_F = 0$ for $\alpha \geq \alpha_c$. Here, α_c is between 1.9 and 2.0. Second, as α increases, the value of τ at which the value of ζ drops to zero decreases. This is a result of the fact that, as α increases, k_r increases at all values of θ, increasing the driving force toward detachment (see Eq. 2). Third, for $\alpha \geq \alpha_c$, $\zeta = 0$ ($\theta = 0$) at a given τ for a given α. In other words, all of the cells detach at the same τ, a result of the fact that fluctuations about θ are not allowed. Hence, typical experimental data which come in the form of the fraction of adherent cells (ζ) as a function of time cannot be easily interpreted with the deterministic formulation (see Part 2 [35]).

Probability density function

In Figs. 7, *a–c*, the probabilistic results for $p(\theta)$ as a function of τ are shown for α equal to 1.8, 1.9, and 2.3, respectively. These results show several interesting trends. Three of the trends are fairly evident and are discussed here (other features are discussed in the following sections, where they are more readily seen). First, the area under the distribution (P_b) becomes fairly constant at larger τ, reaching a "final" or "steady state" value of $P_{b(F)}$. In these figures, $P_{b(F)}$ is 0.79, 0.63, and 0.0, respectively. Here, we should mention that as $\tau \rightarrow \infty$, $p(\theta, \infty) \rightarrow 0$ (33), a result of the assumption that $\theta = 0$ is "absorbing" ($p(0, \tau) = 0$) (33). In other words, after P_b reaches what appears to be a "steady state" value, there is an extremely small, nearly negligible probability loss that continues with τ. Second, at large τ, the maximum in $p(\theta)$, defined as P_m, occurs at $\theta \approx \theta_s$, where θ_s is the stable

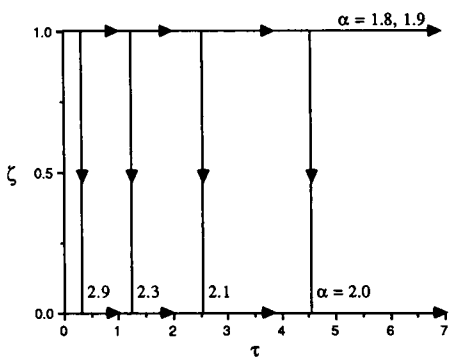

FIGURE 6 Transient results of the deterministic detachment model. The fraction of adherent cells (ζ) is plotted vs. the dimensionless time (τ) at several values of dimensionless force (α). For these analyses, $\kappa = 0.029$; and the initial condition is $\theta = 0.84$.

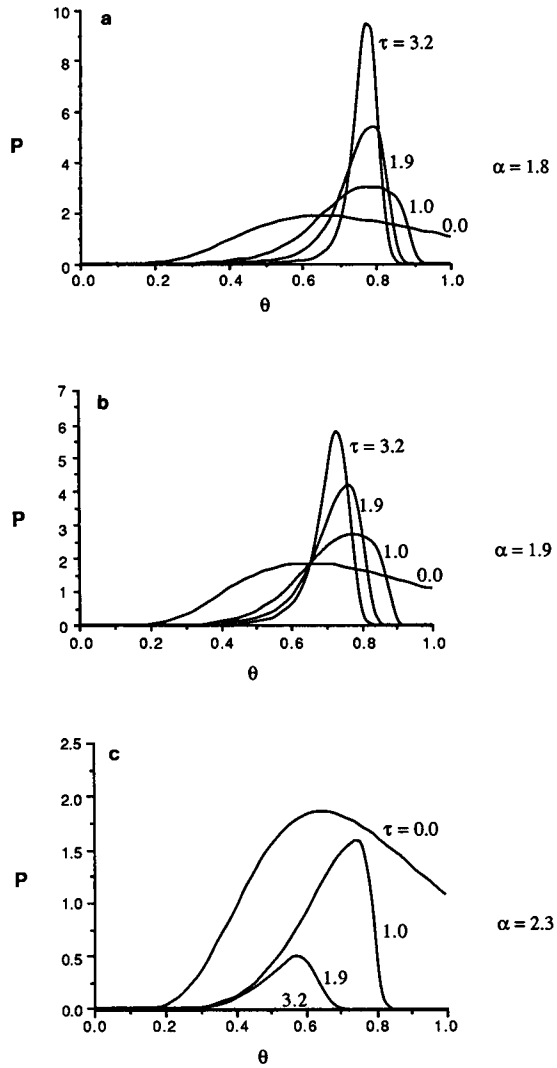

FIGURE 7 Results of the probabilistic analysis of detachment. The probability density function ($p[\theta, \tau]$) is plotted vs. the dimensionless bond number (θ) at several values of dimensionless time (τ). (*a*) The dimensionless force (α) is equal to 1.8; (*b*) 1.9; and (*c*) 2.3. For these analyses, $\kappa = 0.029$; and the initial distribution ($p[\theta, 0]$) is lognormal with $\langle\theta\rangle = 0.84$ and $\sigma^2 = 0.13$.

steady state that is predicted by the deterministic steady state detachment analysis (see Figs. 1 *a* and *b*). Third, P_m (θ_s) and $P_{b(F)}$ decrease as α increases.

Probability of bonds (P_b)

P_b profiles as a function of α are shown in Fig. 8. We defined P_b to be the probability of cell adhesion; therefore, it is equivalent to ζ. Here, we see five trends, some of which are evident in Figs. 7, *a–c* as well. First, probability loss (cell detachment) begins instantaneously, i.e., there is not a lag before the start of detachment. Second, detachment occurs over a range of τ rather than at one particular τ. Third, the dimensionless rate of probability loss (dimensionless detachment rate) decreases with τ, and, consequently, $P_{b(F)}$ appears fairly constant at larger τ. Fourth, $P_{b(F)}$ is a function of α. Fifth, the initial dimensionless detachment rate increases with α. In contrast, the deterministic model predicted that all of the cells detach for $\alpha \geq \alpha_c$, and all of the cells remain attached for $\alpha < \alpha_c$ (see Fig. 6). In addition, it did not allow for fluctuations in θ; therefore, at a given α, all of the cells detach at the same τ, rather than over a range of τ.

The deterministic steady state analysis predicted that certain values of α yield three different zones (see Figs. 1, *a* and *b*). For an initial probability distribution with $\sigma^2 > 0$, we may have probability in all three regions at $\tau = 0$, i.e., cells with a range of θ (see Fig. 7). For $\theta_u < \theta < \theta_s$ and for $\theta_s < \theta < 1.0$ (any cells with $\theta > \theta_u$), the deterministic analysis predicted that the "driving force" is toward the stable steady state (θ_s) and adhesion. For $0 < \theta < \theta_u$ (any cells with $\theta \leq \theta_u$), the "driving force" is toward bond breakage and detachment, in addition, this "driving force" rapidly increases as θ decreases, a result of the exponential term in the expression for k_r (Eq. 2). Here, we use this model to analyze the five trends seen in Fig. 9. First, any cells with very small θ are predicted to detach almost instantaneously. Second, detachment is expected to occur over a range of τ (as θ increases from δ to θ_u, it takes longer to detach). Third, the rate of detachment is predicted to decrease as τ increases, reaching a value of essentially zero for larger values of τ because cells with a driving force toward detachment are removed, leaving those with a driving force toward adhesion. Fourth, the deterministic steady state detachment analysis indicated that as α increases, θ_u increases. This increases the amount of probability with $\theta \leq \theta_u$ at $\tau = 0$, accounting for the fact that $P_{b(F)}$ decreases as α increases. Fifth, as α increases, k_r increases at all values of θ, which increases the detachment rate; therefore, the initial detachment rate is also predicted to increase. This analysis is the deterministic detachment analysis for a probabilistic initial condition. Detachment is, however, also predicted to be probabilistic. Therefore, even if the number of bonds is sufficient for adhesion, there is a continuing probability that the bonds will dissociate and the cell will detach. Likewise, even if the number of bonds is less than that required for adhesion, there is a continuing probability that enough bonds will form and the cell will remain attached. This probabilistic behavior adds to the fluctuations (with respect to the dimensionless time of detachment and fraction of cells that detach) seen in the probabilistic analysis of detachment.

The shape of the P_b profile at a given α depends on the initial probability distribution ($p[\theta, 0]$), in particular, on the variance (σ^2). The profiles in Fig. 8 are typical for combinations of κ and τ_a that give $\sigma^2 > 0$ at $\tau = 0$. Initial

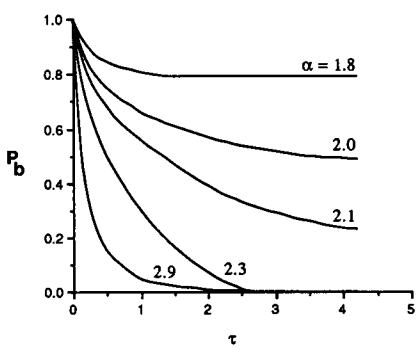

FIGURE 8 A plot of the area (P_b) under the probability density function for detachment vs. dimensionless time (τ) at various values of the dimensionless force (α). These results are typical for initial probability distributions ($p[\theta, 0]$) with $\sigma^2 > 0$; here, $\kappa = 0.029$ and ($p[\theta, 0]$) is lognormal with $\langle\theta\rangle = 0.84$ and $\sigma^2 = 0.13$.

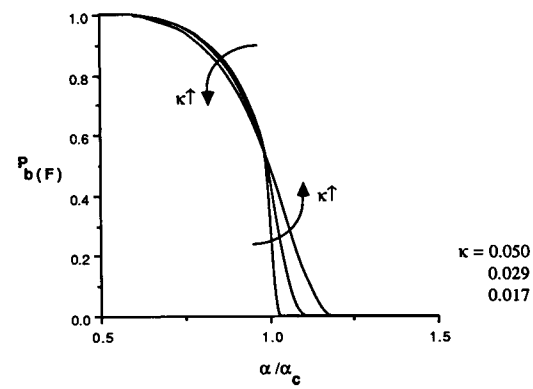

FIGURE 9 A plot of the final value for the area under the probability density function ($P_{b(F)}$) vs. the dimensionless force acting on the bonds (α) divided by the critical value of α (α_c) (where α_c is value at which $P_{b(F)} = 0.5$) at several values of the dimensionless dissociation constant (κ). The results shown are for $k_f^0 N_L$ equal to 0.4, 0.7, and 1.2 min^{-1} with k_r^0 equal to 0.02 min^{-1} (κ equal to 0.050, 0.029, and 0.017, respectively). The initial distribution ($p[\theta, 0]$) is lognormal with $\langle\theta\rangle \approx 0.84$ and $\sigma^2 \approx 0.13$.

distributions with $\sigma^2 \approx 0$, however, yield profiles with a different form. These differences are discussed in detail in Appendix 2. In general, the detachment analyses for $\sigma^2 > 0$ at $\tau = 0$ yield results that are similar to detachment data for model cells in the Radial-Flow Detachment Assay and for cells in other adhesion assays (see Part 2 [35]); therefore, we concentrate on these parameter ranges.

"Final" value of P_b

Figs. 7 and 8 show that $P_{b(F)}$ is a function of α, where $P_{b(F)}$ is equivalent to ζ_F, the "final" fraction of adherent cells. Typically, the critical force exerted on a cell in an adhesion assay is defined as the value at which 50% of the cells detach, i.e., at which $\zeta_F = 0.5$ (22, 47, 48). For consistency, we define the critical value for α (α_c) to be the value at which $P_{b(F)} = 0.5$. In the deterministic analysis, we defined α_c as the smallest value of α for which $\zeta_F = 0$ because either all of the cells are adherent or all of the cells detach, i.e., there is no value of α at which $\zeta_F = 0.5$. In Fig. 9, we show the effect of a change in N_L on $P_{b(F)}$ as a function of α/α_c for $k_f^0 N_L$ equal to 0.4, 0.7, and 1.2 min^{-1} with k_r^0 equal to 0.02 min^{-1} (κ equal to 0.050, 0.029, and 0.017, respectively). Here, we assume that the change in κ is the result of a change in N_L, although the results are the same for a change in k_f^0 and/or N_L. We focus on the effect of N_L because it is relatively simple to vary experimentally and, consequently, it is a key parameter for which data are available. By definition, $P_{b(F)} = 0.5$ at $\alpha/\alpha_c = 1.0$; therefore, all three plots contain this point. The plots in Fig. 9 are somewhat sigmoidal. In contrast, the deterministic model predicted that the detachment curve for ζ_F vs. α would be a step function, with $\zeta_F = 1.0$ at $\alpha < \alpha_c$ and $\zeta_F = 0$ at $\alpha \geq \alpha_c$. The results in Fig. 9 also show that the range of α/α_c over which there is a drop in $P_{b(F)}$ decreases as κ decreases (N_L increases). In addition, these results predict that the value of α_c increases as κ decreases, having a value of ~1.7, 2.0, and 2.3, respectively. Therefore, for a given α, $P_{b(F)}$ increases as κ decreases. This is consistent with predictions of Hammer and Lauffenburger (30) in the "affinity controlled" regime (applicable for low affinity) that the adhesive force increases as the ligand density and/or receptor-ligand affinity constant increase.

Half-life for P_b

Because the value of P_b becomes fairly constant at larger τ, we can characterize a P_b vs. τ plot by its half-life ($\tau_{1/2}$), where $\tau_{1/2}$ is defined as the value for τ at which half of the loss in P_b has occurred, i.e., at which $P_b = 0.5\,(1 + P_{b(F)})$. We define: $\Psi = \tau_{1/2}/\tau_{(1/2)m}$; and $\alpha_m = \alpha(\tau_{(1/2)m})$, where $\tau_{(1/2)m}$ is the maximum value of $\tau_{1/2}$ at a given κ, Ψ is the dimensionless half-life at a given α for a given κ, and α_m is the value of α at which $\tau_{1/2} = \tau_{(1/2)m}$. By definition, $\alpha/\alpha_m = 1.0$ at $\Psi = 1.0$. In addition, $\Psi = 0$ at $\alpha/\alpha_m = 0$ because detachment is negligible so $P_{b(F)}$ is reached instantaneously. The effect of a change in N_L (κ) on Ψ as a function of α/α_m is illustrated in Fig. 10 for the parameter values in Fig. 9. Fig. 10 shows that Ψ increases then decreases as α/α_m increases. In addition, Ψ does not appear to be a strong function of κ (over this range of κ) for $0 < \alpha/\alpha_m < 0.6$ and $1.0 < \alpha/\alpha_m < 1.4$. However, for $0.6 < \alpha/\alpha_m < 1.0$, as κ increases, Ψ increases. As a result, the range of α/α_m over which there are appreciable Ψ values increases as κ increases (N_L decreases). In addition, these results predict that the value of α_m increases as κ decreases, having a value of ~1.9, 2.2, and 2.4, respectively.

A simple explanation for the biphasic dependence of Ψ on α is the following. For small α, the deterministic steady state detachment analysis predicted that θ_u is very small and θ_s decreases only slightly. Therefore, only a small fraction of the cells detach and those detach quickly. In other words, the perturbation is not that significant, and a new steady state is rapidly established. For large α, however, there are no stable steady states. Hence, the driving force is toward detachment for all of the cells. In addition, the larger the value of α, the larger the driving force for detachment (Eq. 2); so, the smaller the half-life. As a result, it is the intermediate values of α that yield larger values for the half-life. As α increases within this intermediate range, θ_u increases, increasing the amount of probability (number of cells) with $\theta < \theta_u$ at $\tau = 0$. This increases the amount of time required for the cells that should detach to detach, increasing the half-life. In addition, because bond formation is probabilistic, cells

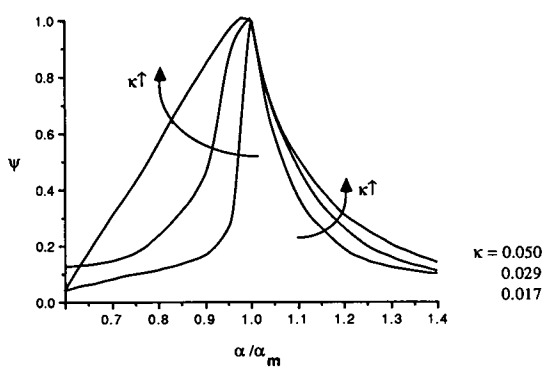

FIGURE 10 A plot of the dimensionless half-life (Ψ) for probability loss vs. the dimensionless force (α) divided by the value of α at which the half-life is maximal (α_m) at several values of the dimensionless dissociation constant (κ). The results shown are for $k_f^0 N_L$ equal to 0.4, 0.7, and 1.2 min^{-1} with k_r^0 equal to 0.02 min^{-1} (κ equal to 0.050, 0.029, and 0.017, respectively). The initial distribution ($p[\theta, 0]$) is lognormal with $\langle\theta\rangle \approx 0.84$ and $\sigma^2 \approx 0.13$.

with $\theta < \theta_u$ may remain attached and cells with $\theta > \theta_u$ may eventually detach. In other words, there is something analogous to a "tug-of-war" about θ_u between attachment and detachment.

Comparison of deterministic and probabilistic analyses

Figs. 6 and 8 show the detachment behavior predicted by the deterministic analysis and by the probabilistic analysis, respectively, at several values of α. The deterministic model predicts that all of the cells detach at a given τ for larger α, whereas the probabilistic model predicts that a portion of the cells detach over a range of τ. These plots can be characterized in terms of τ_{ct}, where τ_{ct} is the value of τ at which $\zeta = 0.5$ (equivalent to the value of τ at which $\zeta = 0$ in the deterministic analysis). In Fig. 11, we compare the deterministic and probabilistic predictions for α as a function of τ_{ct}. (For $\alpha < 1.91$, the deterministic model predicts that $\zeta_F = 1.0$ and the probabilistic model predicts $\zeta_F > 0.5$; therefore, these plots do not extend below this value of α). This figure clearly shows that the deterministic model overestimates the dimensionless time required for detachment for a given level of force, in some ranges by as much as an order of magnitude. The size of the overestimate in dimensional time (t) depends on the value of $k_f^0 N_L$. For example, at $\kappa = 0.029$ and $\alpha = 2.9$, the deterministic model predicts that all of the cells detach at $\tau_{ct} \approx 0.3$, whereas the probabilistic model predicts that 50% of the cells detach by $\tau_{ct} \approx 0.1$. For $k_f^0 N_L \approx 10^{-2}$ min^{-1}, these values of τ_{ct} correspond to 30 and 11 min, respectively; for $k_f^0 N_L \approx 10^6$ min^{-1}, however, these values of τ_{ct} yield 3×10^{-7} and 1×10^{-7} min, respectively.

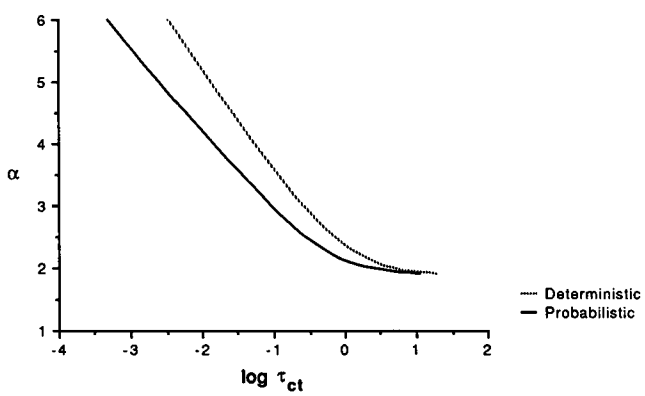

FIGURE 11 Comparison of the deterministic and probabilistic analyses of detachment. Here, we plot the dimensionless force (α) as a function of the dimensionless time (τ_{ct}) at which the fraction of adherent cells (ζ) is 0.5 (zero in the deterministic model). The results shown are for $\kappa = 0.029$. The initial distribution for the probabilistic analyses is lognormal with $\langle\theta\rangle = 0.84$ and $\sigma^2 = 0.13$; and for the deterministic analyses is $\theta(0) = 0.84$.

We define: $\eta = k_r^0 t_{ct}$, where t_{ct} is the time at which $\zeta = 0.5$ (equivalent to the time at which $\zeta = 0$ in the deterministic analysis) and η is the dimensionless critical transient time. Here, we again assume that the change in κ is the result of a change in N_L, the results would, however, be identical for a change in k_f^0 and/or N_L. In Fig. 12, we show the deterministic and probabilistic analyses of α_{ct} as a function of κ for $\eta = 0.02$, where α_{ct} is the value of α at which $\zeta = 0.5$. For a given κ, the initial condition for the deterministic analysis is the steady state value of θ that is predicted by the deterministic attachment model, and the initial distribution for the probabilistic analysis is lognormal with the steady state values of $\langle\theta\rangle$ and σ^2 that are predicted by the probabilistic attachment model (see Eqs. 10 and 11, respectively). The lognormal distribution is used to insure that $p(0, 0) = 0$; however, the use of this distribution limits the range of κ that can be examined with our model to values $< \sim 1$. This limitation results because the detachment behavior cannot be accurately described when the initial probability at small θ is significant, which is the case for large κ. In Fig. 12, therefore, we extrapolate the probabilistic results to examine larger values of κ. This extrapolation can be justified on the basis of the probabilistic attachment analysis of the fraction of adherent cells at steady state (in the absence of fluid stress), which yields values of 0.53 and 0.50 at κ equal to 100 and 1,000, respectively. Therefore, $\alpha_{ct} \approx 0$ at $\kappa > \sim 100$, whereas the deterministic model predicts that $\alpha_{ct} \approx 0.03$ at $\kappa = 100$. In fact, the extrapolation shown on the plot is probably conservative. Fig. 12 shows that the deterministic analysis can overestimate the value of α required to detach the cells. The magnitude of the overestimate depends on the value of κ; at the small end of the range (large $k_f^0 N_L$), it is negligible; at the large end of the range (small $k_f^0 N_L$), however, our extrapolation indicates that the deterministic model can overestimate α_{ct} by over an order of magnitude.

DISCUSSION

We have developed a probabilistic model of receptor-ligand bond formation to describe the probability of receptor-mediated adhesion in a fluid shear field. Our detachment model extends the deterministic model of Hammer and Lauffenburger (30) to a probabilistic framework in which we calculate the probability that a certain number of bonds between a cell and surface exists. A probabilistic framework is used to account for the fluctuations inherent in a chemical reaction involving relatively small numbers of reacting molecules, as is the case with cell surface receptor molecules. We investigate two situations: first, cell attachment in the absence of fluid stress; and, second, cell detachment in the presence of fluid

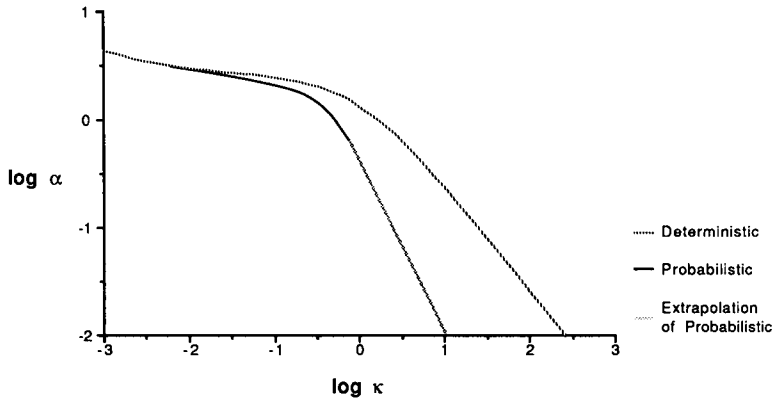

FIGURE 12 Comparison of the deterministic and probabilistic analyses of detachment. Here, we show the deterministic and probabilistic analyses of α_{ct} as a function of the dimensionless dissociation constant (κ) for a dimensionless critical transient time (η) of 0.02, where α_{ct} is the value of α at which $\zeta = 0.5$ (zero in the deterministic model). For a given κ, the initial condition for the deterministic analysis is the steady state value of θ that is predicted by the deterministic attachment model, and the initial distribution for the probabilistic analysis is lognormal with the steady state values of $\langle\theta\rangle$ and σ^2 that are predicted by the probabilistic attachment model. The extrapolatation is explained in the text. Here, the change in κ is assumed to be the result of a change in N_L, the results would, however, be identical for a change in k_f^0.

stress. In the attachment case, we use the expressions developed by McQuarrie (23) to examine the expected variance in bond formation as a function of attachment time; this also provides an initial condition for the detachment case. Focusing then on detachment, we predict transient behavior as a function of key system parameters, such as the distractive fluid force, the receptor-ligand bond affinity and rate constants, and the receptor and ligand densities. Our probabilistic results indicate that deviations from ideal, deterministic cell attachment and detachment behavior can be interpreted in terms of the kinetics. Deviations from ideal attachment and detachment behavior may, however, also result from heterogeneous cell properties, such as receptor number and class (7, 26, 27), and heterogeneous surface properties, such as the presence of several different proteins that each interact with unique cell receptors (28, 29). The lack of quantitative information on these heterogeneities, however, makes it difficult to interpret their role in cell adhesion behavior at this time. In the remainder of this section, we summarize our key results.

The probabilistic analysis of attachment indicates how certain controllable parameters affect the attachment kinetics, in particular, the dimensionless attachment time (τ_a) and the dimensionless dissociation constant (κ). Figs. 2 and 3 show that it is desirable to incubate the cell and the surface for a period of time that is long enough for maximal bond formation ($\langle\theta\rangle$) with minimal variance (σ^2). These figures also indicate that the steady state value for $\langle\theta\rangle$ and σ^2 increase and decrease, respectively, as κ decreases. Therefore, it is advantageous to minimize κ, which can be achieved by capitalizing on a high affinity receptor-ligand interaction and/or by increasing the ligand density. In addition, because θ is normalized to the total number of receptors available for binding (R_T), the number or bonds (C) increases as R_T increases. Therefore, the adhesive force is predicted to increase as the ligand density, receptor density, and/or receptor-ligand affinity increase. These predictions are consistent with those of Hammer and Lauffenburger (30) in the "affinity controlled" regime, applicable for low affinity. The deterministic analysis of attachment predicts identical results for θ as those predicted by the probabilistic model for $\langle\theta\rangle$, there are, however, no fluctuations or deviations about the mean solution, i.e. $\sigma^2 = 0$. As a result, the deterministic analysis underestimates the attachment time required for all of the cells to become attached, where we assume that a cell is currently attached when at least one bond exists ($\theta \geq \delta$) (see Fig. 5).

When attachment efficiency is optimized, the result is maximal adhesive force with minimal variance, crucial for maximal cell adhesion in a fluid shear field. The probabilistic analysis of detachment indicates how certain controllable parameters affect the detachment kinetics, in particular, τ_a, κ, and the dimensionless force acting on the bonds (α). The adhesion efficiency is optimized by maximizing the final fraction of adherent cells. Our probabilistic detachment analysis (Figs. 8, 9, and A1) suggests that this can be achieved through minimization of α (a decrease in the hydrodynamic force and/or an increase in the receptor density), minimization of κ (an increase the ligand density and/or the receptor-ligand affinity), and optimization of τ_a (to maximize the number of bonds and minimize the variance).

In comparing the deterministic and probabilistic detachment predictions, we find that the deterministic model can

yield some inaccurate results. The deterministic model can overestimate the time required for cell detachment at a given α and κ (see Fig. 11) and the dimensionless force required for cell detachment in a given period of time at a given κ (see Fig. 12). The magnitude of these overestimates depends on the value of κ, but it can be significant at large κ (small $k_f^0 N_L$). In addition, the deterministic model predicts that all of the cells detach at a given τ for larger α (see Fig. 6), rather than a portion of the cells over a range of τ (as predicted by the probabilistic model [see Fig. 8]). Hence, typical experimental data which come in the form of the fraction of adherent cells vs. time cannot be easily interpreted with the deterministic model (see Part 2 [35]). Finally, care must be taken in predicting detachment behavior in EC seeding and CAC with a deterministic model because, not only can it overestimate the force necessary for cell detachment, it cannot predict the small amount of detachment that can occur for $\alpha < \alpha_c$, detachment which may ruin the potential success of these processes.

In Part 2 (35), we use our probabilistic models to analyze transient data obtained with a model cell system and the Radial-Flow Detachment Assay. These data provide an important test of this theoretical framework, along with the use of parameter values that are consistent with previous estimates (34). In addition, we compare our probabilistic predictions with transient data on EC seeding of prosthetic vascular grafts, CAC, and cell adhesion reported from other assays, recognizing that rigorous modeling of these data should include physiological effects (such as diffusion of receptors into the contact area with time, time-dependent cell deformability, heterogeneous properties, and a spatially dependent stress distribution within the contact area) beyond our basic model features. Although the theoretical framework used in this paper can, in general, be extended to include these various properties, it proves to be quite insightful in its present form.

APPENDIX 1

Detailed derivation of probabilistic model for detachment

In Eq. 7, we show the expression for the probability of having C complexes at time $t + \Delta t$ [$P_C(t + \Delta t)$] for attachment in the absence of fluid stress. For detachment, we substitute the appropriate expression for the reverse rate constant (Eq. 2) into Eq. 7. In the limit $\Delta t \rightarrow 0$, Eq. 7 (modified for detachment) reduces to the following:

$$\begin{aligned} dP_C/dt = {} & k_f^0 N_L [R_T - (C - 1)] P_{(C-1)} \\ & - [k_f^0 N_L (R_T - C) P_C \\ & + k_r C \exp(\gamma F_T / k_b T C) P_C] \\ & + k_r (C + 1) \exp[\gamma F_T / k_b T (C + 1)] P_{(C+1)}. \end{aligned} \quad (A1)$$

This equation is called the Master equation. Eq. A1 is applicable for $C = 1, 2, \ldots, R_T - 1$. Separate equations are written for the probability of zero bonds and for the probability of R_T bonds, providing us with $R_T + 1$ coupled ordinary differential equations. We put Eq. A1 in dimensionless form and obtain:

$$\begin{aligned} dP_\theta/d\tau = {} & R_T[1 - (\theta - \delta)] P_{(\theta-\delta)} \\ & - \{R_T[(1 - \theta) + \kappa\theta \exp(\alpha/\theta)] P_\theta\} \\ & + \kappa R_T(\theta + \delta) \exp[\alpha/(\theta + \delta)] P_{(\theta+\delta)}. \end{aligned} \quad (A2)$$

We take the limit as $\delta \rightarrow 0$, a reasonable approximation for $R_T \gg 1$. Next, we expand the probabilities and the exponential part of the reverse rate constant in a Taylor's series about P_θ and $\exp(\alpha/\theta)$, respectively. Here, by convention, we neglect terms of order δ^3 (31–33). The resulting equation, a "Fokker-Planck equation," is typically written in the form shown in Eq. 12. It may also be written in terms of the probability current (J) (as shown in Eq. 15), where (33):

$$J = A(\theta) p - (1/2) \partial/\partial\theta [B(\theta) p]. \quad (A3)$$

At $\theta = 1$, we have a reflecting barrier; therefore, the boundary condition is $J(1, \tau) = 0$. Both $A(\theta)$ and $B(\theta)$ are discontinuous at $\theta = \delta$; nevertheless, there is free motion across this point. This discontinuity is a result of the fact that a bond cannot be broken if there is no bond to break (which is the case between $\theta = 0$ and δ). The probability and the current must both be continuous across $\theta = \delta$; therefore $J(\delta+, \tau) = J(\delta-, \tau)$ and $p(\delta+, \tau) = p(\delta-, \tau)$, where evaluation at $\delta+$ and $\delta-$ yield the limits of the quantities from the rhs and the lhs of δ, respectively. Using these criteria, we obtain the boundary condition given in Eq. 16.

APPENDIX 2

Effect of $p(\theta, 0)$ on P_b profiles

The shape of the P_b profile at a given α depends on the initial condition ($p[\theta, 0]$), in particular, on the variance (σ^2). σ^2 is a function of κ and τ_a (Eq. 9). In general, combinations of κ and τ_a that give $\sigma^2 > 0$ yield the profiles shown in Fig. 8; and combinations that give $\sigma^2 \approx 0$ yield the profiles shown in Fig. A1. The analysis shown in Fig. A1 is for $\kappa = 0.0035$; and a lognormal initial distribution ($p[\theta, 0]$) with $\langle\theta\rangle \approx 0.99$ and $\sigma^2 \approx 0.0085$. In Fig. A1, at large values of α: there is a dimensionless time lag before detachment begins, then, as τ increases, all of the cells eventually detach ($P_b = 0$). In addition, as α increases, the dimensionless lag period decreases and the value of τ at which P_b first equals zero decreases. At small values of α ($\alpha \leq 3.4$), P_b remains at ~1. Therefore, a plot of $P_{b(F)}$ vs. α is essentially a step function, as predicted by the deterministic model. The dynamic behavior is, however, different because the deterministic model predicts that all of the cells at a given α detach at one particular τ. Notice that $P_{b(F)} = 1.0$ over the range of α used in Fig. 8.

For $\sigma^2 > 0$, $p(\theta, 0) > 0$ over a large range of θ (see Fig. 7, $\tau = 0$); and for $\sigma^2 \approx 0$, $p(\theta, 0) > 0$ over a very small range of θ, close to $\theta = 1.0$ (see Figs. 2 and 3). The deterministic steady state analysis predicted that certain values of α yield three different regions (Figs. 1, *a* and *b*). For $\sigma^2 > 0$, we may have probability in all three regions at $\tau = 0$; however, for $\sigma^2 \approx 0$, we would expect to have probability in only the first region ($\theta_s < \theta < 1.0$) at $\tau = 0$. Here, therefore, it is not until there are no stable steady states that we begin to see detachment. The lag for detachment is a result of the fact that all of the probability must travel from $\theta \approx 1.0$ to $\theta = 0$. As α increases, the exponential term in the expression for k_r increases at all values for θ (see Eq. 2), which decreases the lag and

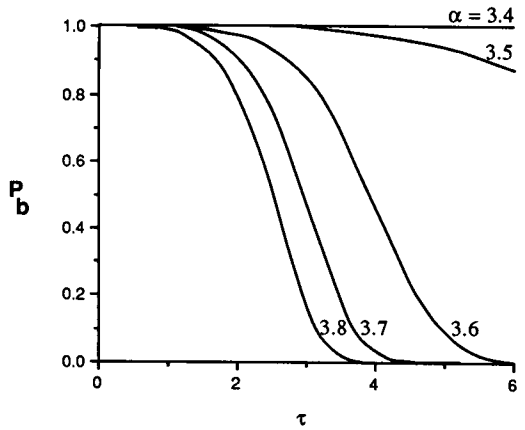

FIGURE A1 A plot of the area (P_b) under the probability density function for detachment vs. dimensionless time (τ) at various values of the dimensionless force (α). These results are typical for initial probability distributions ($p[\theta,0]$) with $\sigma^2 \approx 0$, here, $\kappa = 0.0035$ and ($p[\theta,0]$) is lognormal with $\langle\theta\rangle = 0.99$ and $\sigma^2 = 0.0085$.

increases the detachment rate. This explanation for the two forms of the P_b profiles is based on the deterministic steady state analysis. We must, however, not forget that we are explaining probabilistic results. As a result, all of the probability at a given θ may not move in the direction predicted by the deterministic model. For example, once probability arrives at θ_s, it may not stay there, rather it may fluctuate about this point or move away from it altogether. These deviations from ideal behavior add to the fluctuations seen in the probabilistic analysis of detachment.

The authors wish to thank Daniel Hammer for several helpful conversations and Brian Farrell for helpful discussions on numerical methods.

This work was supported by National Science Foundation grant Emerging Engineering Technology 87-12784 from the Biotechnology Program and by National Institutes of Health Small Business Innovation Research grant AI-26015 to Sepracor, Inc. Financial support from an American Association of University Women Selected Professions Fellowship to C. Cozens-Roberts is also gratefully acknowledged.

Received for publication 22 September 1989 and in final form 11 June 1990.

REFERENCES

1. Atherton, A., and G. V. R. Born. 1972. Quantitative investigations of the adhesiveness of circulating polymorphonuclear leukocytes to blood vessel walls. *J. Physiol.* 222:447–474.
2. Thomas, P. D., F. W. Hampson, and G. W. Hunninghake. 1988. Neutrophil adherence to human endothelial cells. *J. Lab. Clin. Med.* 111:286–292.
3. Berenson, R. J., W. I. Bensinger, D. Kalamasz, F. Schuening, H. J. Deeg, T. Graham, and R. Storb. 1987. Engraftment of dogs with Ia-positive marrow cells isolated by avidin-biotin immunoadsorption. *Blood.* 5:1363–1367.
4. Berenson, R. J., W. I. Bensinger, and D. Kalamasz. 1986. Positive selection of viable cell populations using avidin-biotin immunoadsorption. *J. Immunol. Methods.* 91:11–19.
5. Berenson, R. J., L. J. Levitt, R. Levy, and R. A. Miller. 1984. Cellular immunosorption using monoclonal antibodies. *Transplantation. (Baltimore).* 38:136–143.
6. Berenson, R. J., W. I. Bensinger, D. Kalamasz, and P. Martin. 1986. Elimination of daudi lymphoblasts from human bone marrow using avidin-biotin immunosorption. *Blood.* 67:509–515.
7. Seeger, R. C., D. D. Vo, J. Ugelstad, and C. P. Reynolds. 1986. Removal of neuroblastoma cells from bone marrow with monoclonal antibodies and magnetic immunobeads. *In* Transfusion Medicine: Recent Technological Advances. K. Murawski and F. Peetoom, editors. Alan R. Liss, Inc., New York. 285–293.
8. Kvalheim, G., O. Fodstad, A. Pihl, K. Nustad, A. Pharo, J. Ugelstad, and S. Funderud. 1987. Elimination of B-lymphoma cells from human bone marrow: model experiments using monodisperse magnetic particles coated with primary monoclonal antibodies. *Cancer Res.* 47:846–851.
9. Ramalanjaona, G., R. F. Kempczinski, J. E. Rosenman, C. Douville, and E. B. Silberstein. 1986. The effect of fibronectin coating on endothelial cell kinetics in polytetrafluoroethylene grafts. *J. Vasc. Surg.* 3:264–272.
10. Kesler, K. A., M. B. Herring, M. P. Arnold, J. L. Glover, H. M. Park, M. N. Helmus, and P. J. Bendick. 1986. Enhanced strength of endothelial attachment on polyester elastomer and polytetrafluoroethylene graft surfaces with fibronectin substrate. *J. Vasc. Surg.* 3:58–64.
11. Jarrell, B. E., S. K. Williams, L. Solomon, L. Speicher, E. Koolpe, J. Radomski, R. A. Carabasi, D. Greener, and F. E. Rosato. 1986. Use of an endothelial monolayer on a vascular graft prior to implantation. *Ann. Surg.* 203:671–678.
12. Jarrell, B. E., S. K. Williams, G. Stokes, F. A. Hubbard, R. A. Carabasi, E. Koolpe, D. Greener, K. Pratt, M. J. Moritz, J. Radomski, and L. Speicher. 1986. Use of freshly isolated capillary endothelial cells for the immediate establishment of a monolayer on a vascular graft at surgery. *Surgery. (St. Louis).* 100:392–399.
13. Pratt, K. J., B. E. Jarrell, S. K. Williams, R. A. Carabasi, M. A. Rupnick, and M. A. Hubbard. 1988. Kinetics of endothelial cell-surface attachment forces. *J. Vasc. Surg.* 7:591–599.
14. Rosenman, J. E., R. F. Kempczinski, Y. Berlatzsky, W. H. Pearce, G. R. Ramalanjaona, and H.S. Bjornson. 1985. Bacterial adherence to endothelial-seeded polytetrafluoroethylene grafts. *Surgery.* 98:816–823.
15. Rosenman, J. E., R. F. Kempczinski, W. H. Pearce, and E. B. Siberstein. 1985. Kinetics of endothelial seeding. *J. Vasc. Surg.* 2:778–784.
16. Ramsay, N. K. C., and J. H. Kersey. 1988. Bone marrow purging using monoclonal antibodies. *J. Clin. Immunol.* 8:81–88.
17. Sprent, J., and R. Korngold. 1981. Immunogenetics of graft-versus-host reactions to minor histocompatibility antigens. *Immunol. Today.* 2:189–193.
18. Bongrand, P., and G. I. Bell. 1984. Cell-cell adhesion: parameters and possible mechanisms. *In* Cell Surface Dynamics: Concepts and Models. A. S. Perelson, C. DeLisi, and F. W. Wiegel, editors. Marcel Dekker, Inc., New York. 459–493.
19. McClay, D. R., G. M. Wessel, and R. B. Marchase. 1981. Intercellular recognition: quantitation of initial binding events. *Proc. Natl. Acad. Sci. USA.* 78:4975–4979.
20. Weigel, P. H., R. L. Schnaar, M. S. Kuhlenschmidt, E. Schmell, R. T. Lee, Y. C. Lee, and S. Roseman. 1979. Adhesion of

hepatocytes to immobilized sugars, a threshold phenomenon. *J. Biol. Chem.* 254:10830–10838.

21. Dejana, E., S. Colella, L. R. Languino, G. Balconi, G. C. Corbascio, and P. C. Marchisio. 1987. Fibrinogen induces adhesion, spreading, and microfilament organization of human endothelial cells in vitro. *J. Cell Biol.* 104:1403–1411.
22. Mege, J. L., C. Capo, A. M. Benoliel, and P. Bongrand. 1986. Determination of binding strength and kinetics of binding initiation: a model study made on the adhesive properties of P388D1 macrophage-like cells. *Cell Biophys.* 8:141–160.
23. McQuarrie, D. A. 1963. Kinetics of small systems. I. *J. Chem. Phys.* 38:433–436.
24. McQuarrie, D. A. 1964. Kinetics of small systems. II. *J. Chem. Phys.* 40:2914–2921.
25. Bartholomay, A. F. 1962. A stochastic approach to statistical kinetics with application to enzyme kinetics. *Biochemistry.* 1:223–230.
26. Martin, P. J., E. R. Giblett, and J. A. Hansen. 1982. Phenotyping human leukemic T-cell lines: enzyme markers, surface antigens, and cytogenetics. *Immunogenetics.* 15:385–398.
27. Estrabrook, A., C. L. Berger, R. Mittler, P. LoGerfo, M. Hardy, and R. L. Edelson. 1983. Antigenic modulation of human T-lymphocytes by monoclonal antibodies. *Transplant Proc.* 15:651–656.
28. Pratt, B. M., D. Forn, and J. A. Madri. 1985. Endothelial cell-extracellular matrix interactions. *Ann. N.Y. Acad. Sci.* 460: 274–288.
29. Albelda, S. M., M. Daise, E. N. Levine, and C. A. Buck. 1989. Identification and characterization of cell-substratum adhesion receptors on cultured human endothelial cells. *J. Clin. Invest.* 83:1992–2002.
30. Hammer, D. A., and D. A. Lauffenburger. 1987. A dynamic model for receptor-mediated cell adhesion to surfaces. *Biophys. J.* 52:475–487.
31. Bharucha-Reid, A. T. 1960. Elements of the Theory of Markov Processes and their Applications. McGraw-Hill, New York. 468 pp.
32. Goel, N. S., and N. Richter-Dyn. 1974. Stochastic Models in Biology. Academic Press, New York. 269 pp.
33. Gardiner, C. W. 1983. Handbook of Stochastic Methods for Physics, Chemistry, and the Natural Sciences. Springer-Verlag, New York. 442 pp.
34. Cozens-Roberts, C., J. A. Quinn, and D. A. Lauffenburger. 1990. Receptor-mediated adhesion phenomena: model studies with the Radial-Flow Detachment Assay. *Biophys. J.* 58:107–125.
35. Cozens-Roberts, C., J. A. Quinn, and D. A. Lauffenburger. 1990. Receptor-mediated cell attachment and detachment kinetics II. Experimental model studies with the Radial-Flow Detachment Assay. 58:857–872.
36. Bell, G. I. 1978. Models for the specific adhesion of cells to cells. *Science* (*Wash. DC*). 200:618–627.
37. Schmid-Schoenbein, G. W., Y. Fung, and B. W. Zweifach. 1975. Vascular endothelium-leukocyte interactions: sticking shear force in venules. *Circ. Res.* 36:173–184.
38. Evans, E. A. Detailed mechanics of membrane-membrane adhesion and separation. II. Discrete kinetically trapped molecular cross-bridges. *Biophys. J.* 48:185–192.
39. Dembo, M., D. C. Torney, K. Saxman, and D. Hammer. 1988. The reaction-limited kinetics of membrane-to-surface adhesion and detachment. *Proc. R. Soc. Lond. B.* 234:55–83.
40. Derrick, W. R., and S. I. Grossman. 1981. Elementary Differential Equations with Applications. Addison-Wesley Publishing Co., Reading, MA. 532 pp.
41. Bell, G. I., M. Dembo, and P. Bongrand. 1984. Cell adhesion: competition between nonspecific repulsion and specific bonding. *Biophys. J.* 45:1051–1064.
42. Drake, A. W. 1967. Fundamentals of Applied Probability Theory. McGraw-Hill, New York. 283 pp.
43. Ames, W. F. 1977. Numerical Methods for Partial Differential Equations. Thomas Nelson and Sons, New York. 365 pp.
44. Douglas, J., and B. F. Jones. 1963. On Predictor-Corrector Methods for Nonlinear Parabolic Differential Equations. *J. Soc. Indust. Appl. Math.* 11:195–204.
45. Breiman, L. 1973. Statistics: With a View Toward Applications. Houghton Mifflin Co., Boston. 399 pp.
46. Thomas, G. B., Jr., and R. L. Finney. 1980. Calculus and Analytical Geometry. Addison-Wesley Publishing Co., Reading, MA. 891 pp.
47. Capo, C., F. Garrouste, A. Benoliel, P. Bongrand, A. Ryter, and G. I. Bell. 1982. Concanavalin-A-mediated thymocyte agglutination: a model for a quantitative study of cell adhesion. *J. Cell Sci.* 56:21–48.
48. Bongrand, P., C. Capo, A. M. Benoliel, and R. Depieds. 1979. Evaluation of intercellular adhesion with a very simple technique. *J. Immunol. Methods.* 28:133–141.
49. Rutishauser, U., and L. Sachs. 1975. Receptor mobility and the binding of cells to lectin-coated fibers. *J. Cell Biol.* 66:76–85.
50. Sung, K-L.P., L. A. Sung, M. Crimmins, S. J. Burakoff, and S. Chien. 1986. Determination of junction avidity of cytolytic T cell and target cell. *Science* (*Wash. DC*). 234:1405–1408.
51. Lauffenburger, D., and C. DeLisi. 1983. Cell surface receptors: physical chemistry and cellular regulation. *Int. Rev. Cytol.* 84:269–302.
52. Wiegel, F. W. 1984. Diffusion of proteins in membranes. *In* Cell Surface Dynamics: Concepts and Models. A. S. Perelson, C. DeLisi, and F. W. Wiegel, editors. Marcel Dekker, Inc., New York. 135–150.
53. Sklar, L. A. 1987. Real-time spectroscopic analysis of receptor-ligand dynamics. *Ann. Rev. Biophys. Chem.* 16:479–506.
54. Wiley, H. S. 1985. Receptors as models for the mechanisms of membrane protein turnover and dynamics. *Curr. Top. Membr. Transp.* 24:369–412.